Tissue Eng Regen Med (2020) 17(6):801–813
https://doi.org/10.1007/s13770-020-00242-y

Online ISSN 2212-5469 TERM

ORIGINAL ARTICLE

Glucose Uptake and Insulin Response in Tissue-engineered Human Skeletal Muscle

Megan E. Kondash[1] · Anandita Ananthakumar[1] · Alastair Khodabukus[1] · Nenad Bursac[1] · George A. Truskey[1]

Received: 27 October 2019 / Revised: 19 January 2020 / Accepted: 21 January 2020 / Published online: 21 March 2020

Abstract

BACKGROUND: Tissue-engineered muscles ("myobundles") offer a promising platform for developing a human in vitro model of healthy and diseased muscle for drug development and testing. Compared to traditional monolayer cultures, myobundles better model the three-dimensional structure of native skeletal muscle and are amenable to diverse functional measures to monitor the muscle health and drug response. Characterizing the metabolic function of human myobundles is of particular interest to enable their utilization in mechanistic studies of human metabolic diseases, identification of related drug targets, and systematic studies of drug safety and efficacy.

METHODS: To this end, we studied glucose uptake and insulin responsiveness in human tissue-engineered skeletal muscle myobundles in the basal state and in response to drug treatments.

RESULTS: In the human skeletal muscle myobundle system, insulin stimulates a 50% increase in 2-deoxyglucose (2-DG) uptake with a compiled EC_{50} of 0.27 ± 0.03 nM. Treatment of myobundles with 400 μM metformin increased basal 2-DG uptake 1.7-fold and caused a significant drop in twitch and tetanus contractile force along with decreased fatigue resistance. Treatment with the histone deacetylase inhibitor 4-phenylbutyrate (4-PBA) increased the magnitude of insulin response from a 1.2-fold increase in glucose uptake in the untreated state to a 1.4-fold increase after 4-PBA treatment. 4-PBA treated myobundles also exhibited increased fatigue resistance and increased twitch half-relaxation time.

CONCLUSION: Although tissue-engineered human myobundles exhibit a modest increase in glucose uptake in response to insulin, they recapitulate key features of in vivo insulin sensitivity and exhibit relevant drug-mediated perturbations in contractile function and glucose metabolism.

Keywords Tissue engineering · Muscle · Skeletal · Insulin · Myobundles

Abbreviations

2-DG	2-deoxyglucose
4-PBA	4-phenylbutyrate, histone deacetylase inhibitor
ACA	6-aminocaproic acid
AMPK	5′AMP-activated protein kinase
C2C12	A line of mouse myoblasts
DMEM	Dulbecco's Modified Eagle Medium
ECL	Enhanced chemiluminescent
EGF	Epidermal growth factor
GLUT1	Glucose transporter responsible for constitutive glucose uptake

Electronic supplementary material The online version of this article (https://doi.org/10.1007/s13770-020-00242-y) contains supplementary material, which is available to authorized users.

✉ George A. Truskey
george.truskey@duke.edu

[1] Department of Biomedical Engineering, Duke University, Durham, NC 27708, USA

GLUT3	Glucose transporter most often expressed in neurons
GLUT4	Glucose transporter responsible for insulin-mediated glucose uptake
HDAC	Histone deacetylase
HRP	Horseradish peroxidase
hGM	Human growth media
IRS-1/ PI3K/Akt	Insulin receptor substrate (IRS)-1 is a signaling molecule that after activation interacts with phosphoinositide 3-kinase (PI3K) and serine/threonine protein kinases to regulate GLUT4
LAA	Low amino acid
MHC	Myosin heavy chain protein
MYH1	Fast twitch type IIX MHC
MYH3	Immature embryonic form of MHC
MYH7	Slow twitch type I MHC
MYH8	Perinatal isoform of MHC
qRT-PCR	Quantitative reverse transcription polymerase chain reaction
TBST	Tris-buffered saline and 0.1% Tween 20 solution
PGC-1α	Peroxisome proliferator-activated receptor-γ coactivator-1α is a transcriptional coactivator involved in cellular energy metabolism

1 Introduction

Skeletal muscle is responsible for movement and force generation in the human body, comprises nearly 40% of the body's total mass [1], and is exposed to drug metabolites in the bloodstream as a result of its rich vascular network [2]. Most in vitro models of human skeletal muscle rely on traditional two-dimensional (2D) cell cultures which lack the three-dimensional structural and mechanical guidance cues experienced by native tissues in vivo. This results in myotube detachment a few days after fusion of myoblasts, preventing longer-term experimental studies and limiting the developmental maturation of cells [3]. Three-dimensional tissue-engineered skeletal muscles improve upon 2D models by enabling longer-term culture, exhibiting unidirectional aligned fibers similar to those comprising muscle in vivo, and offering the capacity to undergo additional functional tests including measures of contractile function, oxygen consumption, metabolite production, and calcium handling [4–7]. The ability of tissue-engineered human skeletal muscle ("myobundles") to replicate expected isometric contractile properties and native muscle structure has been well characterized [4]. These attributes position human myobundles as a promising tool for studying drug efficacy and toxicity, as well as for elucidating underlying mechanisms of disease pathology to guide targeted drug development [8]. Additionally, the use of human cells enables the study of human-specific drug efficacy and toxicity that may not be detected in animal studies and offers the ability to better model the genetic diversity of human populations [4]. Importantly, these bioengineered platforms have the potential to improve the process of testing drug safety and efficacy.

Skeletal muscle is highly metabolically active and is responsible for 75% of post-prandial glucose uptake [9]. Post-prandial skeletal muscle glucose uptake occurs due to pancreatic β-cell insulin secretion that results in activation of the insulin receptor substrate-1/phosphoinositide 3-kinase/Akt (IRS-1/PI3K/Akt) pathway and consequent translocation of the insulin-sensitive glucose transporter 4 (GLUT4) to sarcolemma [10, 11]. In tissue-engineered muscle formed using mouse C2C12 cell lines, insulin responsiveness [12] as well as the impact of media composition [13, 14], electrical stimulation [15], and cell source [16] on metabolic phenotype have been examined. In tissue-engineered human myobundles, the impact of electrical stimulation on metabolic flux has been characterized [7]. Cells in the myobundles engage in cell–cell and cell-extracellular matrix interactions while being exposed to alignment-promoting passive tension, all of which provide environmental cues that are absent or limited in monolayer culture. Because such environmental cues have the capacity to influence skeletal muscle differentiation, function, and metabolism [17–20], it is possible that glucose uptake and insulin responsiveness may differ between three-dimensional myobundles and two-dimensional monolayer cultures.

Metformin is commonly prescribed as the medication for the first-line treatment of hyperglycemia in type 2 diabetes and acts in part to promote increased glucose uptake in skeletal muscle. Metformin acts by disrupting the function of complex I in the electron transport chain, leading to activation of the 5′AMP-activated protein kinase (AMPK) pathway [21, 22] and by AMPK-independent pathways [23].

Because myotubes cultured in vitro tend to be immature, with low levels of adult myosin heavy chain isoforms and high levels of embryonic and neonatal myosin heavy chain isoforms [24], the general histone deacetylase (HDAC) inhibitor 4-phenylbutyrate (4-PBA) may promote maturation of myotubes in myobundles. Class IIa HDACs include HDAC4, 5, 7, and 9 and are highly involved in the regulation of myogenesis via their interactions with the transcription factor MEF2 [25]. During differentiation of myoblasts to myotubes, these HDACs are exported from the nucleus to the cytoplasm, and overexpression of HDAC4, 5, and 7 prevents myoblasts from differentiating in vitro [26–28]. HDACs also play a role in metabolic

regulation; HDAC4 is exported from the nucleus when skeletal muscle fibers are reprogrammed from glycolytic fiber types to more oxidative fiber types [29] and the general class IIa HDAC inhibitor Scriptaid has been shown to increase metabolic gene expression and oxidative metabolism in rats in a manner similar to exercise [30].

In this study, we examined the ability of insulin to stimulate glucose uptake in human myobundles by determining a dose response to a range of insulin concentrations in order to calculate insulin responsiveness and insulin sensitivity. To determine how the three-dimensional environment in myobundles impacts insulin responsiveness, we measured changes in glucose uptake in response to a physiological insulin concentration of 10 nM in both three-dimensional myobundles and in myotubes in two-dimensional monolayer culture. Next, we validated the ability of the myobundles to recapitulate relevant functional responses to therapeutics using metformin. In addition to its impact on glucose uptake rates, we determined the effect of metformin treatment on myobundle contractile function and gene expression of glucose transporters and myosin heavy chain (MHC) isoforms. Finally, we examined the impact of treatment with the HDAC inhibitor 4-PBA on myobundle metabolic and contractile function.

2 Materials and methods

2.1 Isolation and monolayer culture of primary myoblasts and myotubes

Primary human myogenic cells were isolated from surgical waste samples obtained according to a Duke IRB-approved protocol. Briefly, muscle tissue was rinsed with 2X Antibiotic–Antimycotic (ThermoFisher Scientific, Waltham, MA, USA) in Dulbecco's phosphate buffered saline (DPBS) (Sigma-Aldrich, St. Louis, MO, USA), then minced and incubated with 0.05% Trypsin–EDTA (ThermoFisher Scientific). Minced tissue underwent a 2-hour pre-plating step in an uncoated tissue culture flask before being transferred to a Matrigel (Corning, Corning, NY, USA)-coated flask for the cell outgrowth process. During outgrowth, cells were maintained in human growth media (hGM) containing low glucose (5.55 mM glucose) Dulbecco's modified eagle medium (DMEM) with 1 mM sodium pyruvate (ThermoFisher Scientific) supplemented with 9% fetal bovine serum (FBS) (Hyclone, Logan, UT, USA), 0.25 μg/mL amphotericin B (ThermoFisher Scientific), 50 μg/mL gentamicin (ThermoFisher Scientific), 0.4 μg/mL dexamethasone (Sigma-Aldrich), 10 ng/mL epidermal growth factor (EGF) (Peprotech, Rocky Hill, NJ, USA), and 50 μg/mL fetuin (Sigma-Aldrich).

For monolayer myotube culture, myoblasts were plated at a density of 20,000 cells/cm^2 in a 6-well plate coated with growth-factor reduced Matrigel (Corning). Myoblasts were cultured in hGM for 4 days, then switched to differentiation media for two weeks of differentiation prior to endpoint testing. The plating density was chosen such that cells would be confluent by day 4 of culture and result in approximately the same number of cells by day 4 as were added to myobundles. Differentiation media, referred to as low amino acid (LAA) media, consisted of a custom-formulated low amino acid base media (ThermoFisher Scientific) (Supplementary Table S1) containing 2% horse serum (Hyclone), 25 μg/mL gentamicin (ThermoFisher Scientific), 0.125 μg/mL amphotericin B (ThermoFisher Scientific), 100 μM L-carnitine (Sigma-Aldrich), 0.05% bovine serum albumin (BSA) (ThermoFisher Scientific), 5.55 mM D-glucose (ThermoFisher Scientific), 0.2 mM sodium pyruvate (ThermoFisher Scientific), 2 mM glutamine (ThermoFisher Scientific), 2 mg/mL 6-aminocaproic acid (ACA) (Sigma-Aldrich), 10 nM insulin (Sigma-Aldrich) during week 1 of differentiation and 0 nM insulin during week 2 of differentiation, 50 μM oleate (Sigma-Aldrich) and 50 μM palmitate (Sigma-Aldrich) in a 1:1 mixture complexed to 0.17% bovine serum albumin (Sigma-Aldrich).

2.2 Myobundle formation and culture

Myobundles were formed as previously described [4, 5]. Briefly, cells were suspended in a solution of Matrigel (Corning) and bovine fibrinogen (Sigma-Aldrich) in PBS and polymerized with 50 U/mL thrombin (Sigma Aldrich) while in the central channel of a PDMS mold surrounded by a nylon (Cerex Advanced Fabrics, Cantonment, FL, USA) frame. Each myobundle contained 750,000 cells. After 30 min of polymerization at 37 °C, hGM containing 1.5 mg/mL 6-aminocaproic acid (Sigma-Aldrich) (hGM + ACA) was added to the wells containing the myobundles in the molds. After culture in hGM + ACA for four days, myobundles were taken out of molds and cultured in differentiation media as specified in the previous section, with the exception that myobundles used for the insulin dose response curve shown in Fig. 1 were cultured in differentiation media containing 1.72 μM insulin during week 1 of differentiation and 0 μM insulin during week 2 of differentiation. This higher concentration of insulin was lowered to 10 nM for subsequent experiments to improve the physiologic relevance of culture conditions after it was determined there was no effect of the change on myobundle force production or insulin-stimulated glucose uptake. All myobundles were differentiated for two weeks prior to endpoint testing. In 2D culture, the myoblasts fuse to form multi-nucleated, elongated, primarily spindle-

A

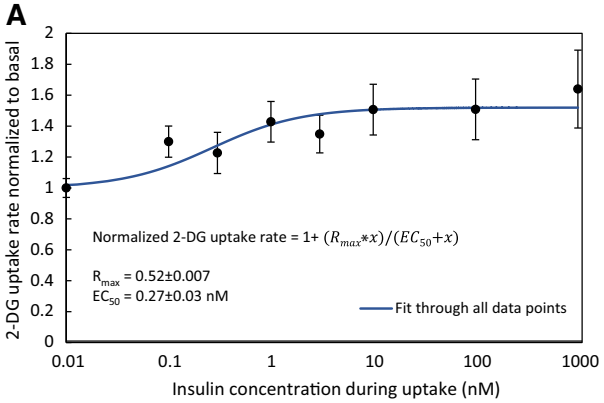

B

Donor	Maximum fold-change in 2-DG uptake	Insulin concentration of maximum response (nM)	R_{max} parameter	EC_{50} parameter (nM)
S110	2.28	10	1.06 ± 0.03	0.87 ± 0.13
S111	1.20	0.05	N/A	N/A
S113	1.40	0.3	0.24 ± 0.02	0.01 ± 0.02
S115	1.95*; 3.39	1*; 1000	1.43 ± 0.03	2.06 ± 0.23
Compiled	1.51*; 1.64	10* ; 1000	0.52 ± 0.01	0.27 ± 0.03

Fig. 1 Characterization of insulin sensitivity and dose response in myobundles. **A** Basal and insulin-mediated 2-DG uptake were measured in myobundles at 2 weeks post-differentiation. The 2-DG uptake rates were normalized to the basal uptake rate for each donor. Using a curve fitting tool, the values for the R_{max} and EC_{50} parameters were determined. **B** Individual donor experimental values for the maximum fold-change in 2-DG uptake with insulin stimulation and the insulin concentration at which that maximum fold-change occurred, as well as the individual donor R_{max} and EC_{50} values. Donor S111 exhibited glucose uptake rates in response to insulin stimulation that were lower than the basal 2-DG uptake, which precluded the determination of the EC_{50} and R_{max} values for that donor. The numbers denoted with * represent values obtained when limiting analysis to only physiologically-relevant insulin concentrations of $\leq$ 10 nM, while the un-starred numbers represent values obtained when considering the full range of insulin doses. For each donor, 2-DG uptake was obtained for n = 3–7 myobundles per insulin concentration. Data presented as mean ± S.E.M

shaped striated myotubes. The myotubes align with each other locally, but at a global scale across the surface of the well plate they orient randomly. The myotube shape in these cultures is often wide and branched. In 3D culture, the myoblasts also fuse to form multi-nucleated, striated myotubes, but these myotubes align in a unidirectional manner along the length of the myobundle and rarely attain a wide or branched shape as would be seen in 2D culture.

2.3 Quantification of 2-deoxyglucose uptake

Measurement of 2-deoxyglucose (2-DG) uptake was achieved using a modified version of the published protocol [31]. After differentiating for 2 weeks, myotubes in monolayer and myobundles were maintained in serum- and insulin-free differentiation media for 18 h prior to uptake measurement. Next, myotubes and myobundles were incubated in uptake buffer composed of 0 mM glucose DMEM (ThermoFisher Scientific) with 0.1% (w/v) bovine serum albumin (Sigma-Aldrich) and 0.2 mM sodium pyruvate for 10 min. Myotubes and myobundles were then acutely stimulated with different concentrations of insulin in fresh uptake buffer for 30 min. Next, myotubes and myobundles (excluding negative control myobundles) were incubated for 20 min in uptake buffer containing the specified amount of insulin and supplemented with 5 mM 2-DG (Sigma-Aldrich). At the conclusion of the uptake period, ice-cold DPBS was used to wash myobundles 3 times. Myobundles were then cut from the frames and lysed in 100 µl of 1 × extraction buffer (Abcam) overnight at 4 °C on a rocker. Following uptake, myotubes were washed with ice-cold DPBS and trypsinized prior to lysis in the same manner as the myobundles. The following day, samples were frozen at − 80 °C, then heated at 85 °C for 40 min to remove endogenous NADP, and 50 µL of 200 mM triethanolamine (TEA) buffer (Sigma-Aldrich) was added to each sample. Samples were kept at − 20 °C until quantification. To quantify the 2-DG6P in the lysed samples, the protocol was followed as put forth in the previous publication [31].

2.4 EC_{50} curve fitting

The 2-DG uptake of myobundles was measured in response to 7–9 different insulin concentrations in order to construct a curve showing the effect of insulin concentration on 2-DG uptake. All uptake rates were normalized to the basal uptake rate within each donor. Using Matlab's curve fitting tool, and the assumption that the effect of insulin on 2-DG uptake follows Michaelis–Menten kinetics, the equation $f(x) = 1 + \frac{R_{max}x}{EC_{50}+x}$, was fitted to the data for each donor where x represents insulin concentration and f(x) represents 2-DG uptake rate normalized to basal uptake rate. To obtain the compiled R_{max} and EC_{50} values, the curve was fitted using all of the normalized 2-DG uptake rates from all donors.

2.5 Contractile function measurements

Contractile force production by myobundles was measured using a setup in which the myobundle frame was pinned to a fixed PDMS slab on one end and attached to a force transducer on the other end [4]. Myobundles were stretched to 115% of normal length prior to electrical stimulation. Twitch force was obtained using a 1 Hertz stimulus for 1 s, tetanus force was obtained using a 20 Hertz stimulus for 1 s, and fatigue force was obtained using a 20 Hertz

stimulus for 30 s. Peak twitch and tetanus force, percent fatigue and twitch kinetics (time to peak twitch and half-relaxation time) were calculated using a Matlab script. Twitch and tetanus forces were calculated as the difference between the highest measured force after stimulation and the baseline passive force prior to stimulation. Percent fatigue was calculated as $\frac{peak\,force - force\,after\,30\,seconds\,of\,fatigue}{peak\,force - baseline\,force} \times 100\%$. Twitch time to max was determined as the time between onset of electrical stimulation and peak force. Twitch half-relaxation time was calculated as the time between peak force and return to one-half of the difference between the peak force and the baseline force.

2.6 Drug treatment

For experiments testing the effect of metformin, myobundles were treated with 400 μM metformin (Sigma-Aldrich) for 18 h prior to the endpoint assays of 2-DG uptake and force testing. The general HDAC inhibitor 4-PBA (Sigma-Aldrich) was added to myotubes and myobundles at a final concentration of 5 mM for 18 h prior to 2-DG uptake.

2.7 qRT-PCR

Myobundles were flash frozen in liquid nitrogen prior to total RNA extraction using the Aurum Total RNA Mini Kit from BioRad. cDNA was produced using the iScript cDNA Synthesis Kit (BioRad). Genes of interest were amplified and quantified using the iQ SYBR Green Supermix (BioRad) and CFX Connect Real-Time PCR Detection System (BioRad). Primer sequences are included in Supplementary Table S2.

2.8 Western blotting

For each treatment condition within a donor, 2–3 samples, each consisting of three pooled myobundles, were flash frozen in liquid nitrogen prior to lysis at 4 °C in RIPA buffer (Sigma-Aldrich) supplemented with phosphatase and protease inhibitor (ThermoFisher Scientific). Samples were homogenized during lysis, centrifuged, and the supernatant was collected and stored at -80 °C. Laemmli sample buffer (Bio-Rad, Hercules, CA, USA) was added to samples, and samples were heated at 37 °C for 10 min prior to gel electrophoresis using a 10% polyacrylamide gel (Bio-Rad). Proteins were then transferred to a Polyvinylidene difluoride (PVDF) membrane. Membranes were blocked at room temperature for 1 h with 5% milk diluted in 1x tris-buffered saline and 0.1% Tween 20 (TBST) (Bio-Rad), then incubated with the appropriate primary antibody diluted in 5% milk overnight at 4 °C. After primary antibody incubation, membranes were washed with TBST and incubated with the appropriate secondary antibody for 45 min at room temperature. Finally, membranes were rinsed with TBST. Proteins were visualized after the addition of an enhanced chemiluminescent (ECL) horseradish peroxidase (HRP) substrate (ThermoFisher Scientific) using a Chemi-Doc Gel Imaging System (Bio-Rad). For each sample, the intensity of the band for the protein of interest was normalized to the intensity of the GAPDH band. Analysis was done using Image Lab Software (Bio-Rad).

2.9 Normalization and statistical analysis

For experiments done with multiple donors, a global normalization process was used for each functional measure (twitch force, tetanus force, 2-DG uptake rate, etc.) to account for inherent differences between the functional output values of myobundles from each donor. A global average was determined, equivalent to the average of all raw output values from all conditions and all donors. Next, a donor-specific average was determined from all conditions within the experiment done using that donor. For each donor, a multiplier consisting of the ratio of the global average to the donor-specific average was propagated through the raw data. Finally, the normalized donor-specific averages for all donors for each condition were averaged to obtain the compiled average for that condition. This method preserves the relative differences in output between conditions within donors while removing differences in background output between donors.

For experiments with multiple donors, the number of donors was used to determine standard error of the mean (S.E.M.) and individual donor averages were used for statistical analysis. For experiments with only one donor, the number of myobundles per condition was used to determine S.E.M., and individual myobundle data were used for statistical analysis. Student's t test was used for pairwise comparisons. For multiple comparisons an ANOVA was run, followed by Tukey HSD post hoc testing for statistical significance. One symbol indicates $p < 0.05$, two symbols indicate $p < 0.01$, and three symbols indicate $p < 0.001$.

3 Results

First, we established the dose response relationship between insulin and increases in glucose uptake to determine the concentration at which insulin-stimulated glucose uptake is half-maximal (EC_{50}) in human myobundles. Curve fitting of the compiled results from insulin dose response experiments in four donors indicated an overall

R_{max} value of 0.52 ± 0.007, which corresponds to a maximum 1.52-fold magnitude of insulin response (where magnitude of insulin response refers to the ratio of insulin-stimulated to basal 2-DG uptake), and an EC_{50} of 0.27 ± 0.03 nM insulin (Fig. 1A). Individual donor R_{max} values were 1.06 ± 0.03, 0.24 ± 0.02, and 1.43 ± 0.03, with EC_{50} values of 0.87 ± 0.13, 0.01 ± 0.02 and 2.06 ± 0.23, respectively (Fig. 1B). One donor (S111) yielded several insulin response values that were lower than the basal 2-DG uptake, which precluded the determination of the EC_{50} and R_{max} values for that donor. When examining only physiological concentrations of insulin of ≤ 10 nM [32], the maximum experimentally measured average magnitude of insulin response 1.5 ± 0.2 and occurred at 10 nM insulin (Fig. 1B). Among all data, the maximum experimentally measured average magnitude of insulin response was 1.6 ± 0.3, occurring at 1000 nM. This was heavily influenced by one donor (S115), which exhibited a large response to 1000 nM insulin (Fig. 1B). All other donors responded maximally to 10 nM insulin or less.

To determine if insulin-stimulated glucose uptake is affected by 3D culture in myobundles, we next compared the magnitude of insulin response in 2D monolayers and 3D myobundles from five independent donors (Fig. 2). When experiments from all donors are compiled, myobundles exhibit a statistically significant higher magnitude of insulin response to 10 nM insulin (2D myotubes: 1.14 ± 0.04 vs 3D myobundles: 1.5 ± 0.1, $p < 0.05$) (Fig. 2).

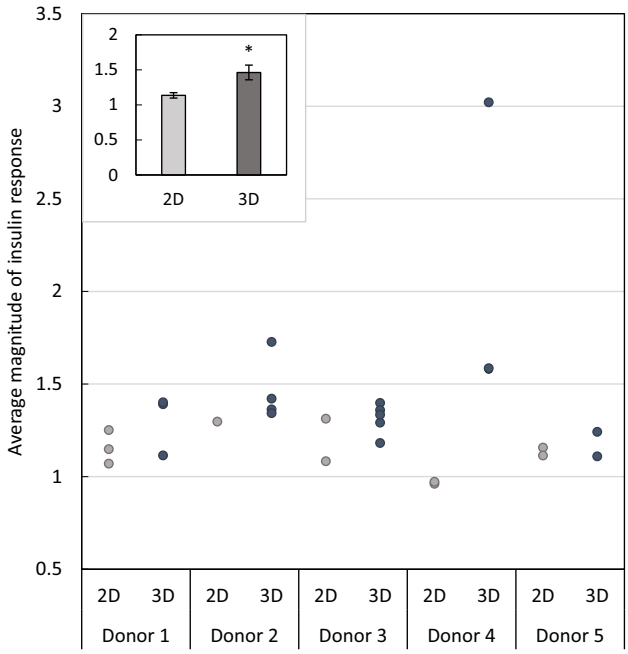

Fig. 2 Compilation of insulin responsiveness in 2-D and 3-D. Data are compiled from experiments shown in this study. The magnitude of insulin response is calculated as a ratio of 2-DG uptake in response to 10 nM insulin over the 2-DG uptake in response to 0 nM insulin (where a magnitude of 1 indicates equivalent uptake rates at 0 and 10 nM insulin). Each data point is obtained by averaging the responses of 3-4 wells (for 2-D) or myobundles (for 3-D), The inlayed graph depicts the average magnitude of insulin response of myotubes in 2-D culture and myobundles in 3-D culture from all donors, shown as mean ± S.E.M

To examine the ability of the myobundle system and 2D myotubes to detect alterations in glucose metabolism due to pharmacological treatment, we treated both myotubes in monolayer culture and myobundles with metformin. A concentration of 400 μM metformin was chosen based on evidence that this concentration elicited a near-maximal increase in glucose uptake in human myotubes in monolayer culture [33]. Both myotubes in 2-dimensional culture (Fig. 3A) and myobundles (Fig. 3B) exhibited a statistically significant increase in glucose uptake in response to metformin treatment. In the absence of insulin, metformin treatment increased the average 2-DG uptake rate of myotubes from 8.3 ± 1.4 nmol/h to 17.0 ± 0.7 nmol/h, a fold-change of 2.0. In myotubes in the presence of insulin, metformin increased the average 2-DG uptake rate from 9.2 ± 0.8 nmol/h to 17.6 ± 1.5 nmol/h, a fold-change of 1.9. In myobundles in the absence of insulin, metformin treatment increased the average 2-DG uptake rate from 8.0 ± 0.7 to 13.6 ± 0.2 nmol/h, a fold-change of 1.7. In the presence of insulin, metformin increased the average 2-DG uptake rate of myobundles from 9.6 ± 0.9 nmol/h to 16.9 ± 1.1 nmol/h, a fold-change of 1.8. Additionally, we examined the impact of metformin treatment on contractile function and observed a statistically significant 35% decrease in twitch force and 29% decrease in tetanus force production in the treated group (Fig. 3C), and a significant increase in fatigue (Fig. 3D) without changes in twitch kinetics (Fig. 3E).

To examine whether changes in glucose transporter or metabolic regulator PGC-1α (peroxisome proliferator-activated receptor-γ coactivator) expression were associated with the changes in myobundle function, we analyzed differences in expression between the no treatment and metformin treated myobundles. Metformin treatment elicited no effect on GLUT4 gene expression, while significantly lowering gene expression of GLUT1 and GLUT3 and increasing expression of PGC-1α (Fig. 4A). Upon assessing the relative abundance of the glucose transporters in the myobundles by normalizing to the expression level of the housekeeping gene, GLUT1 was expressed at much higher levels than GLUT4, and GLUT3 was expressed at levels comparable to those of GLUT1 (Fig. 4B). Metformin treatment significantly lowered expression of the perinatal isoform of myosin heavy chain (MYH8) (Fig. 4C). Interestingly, the myobundles expressed slow twitch type I MHC (MYH7) most abundantly of the MHC

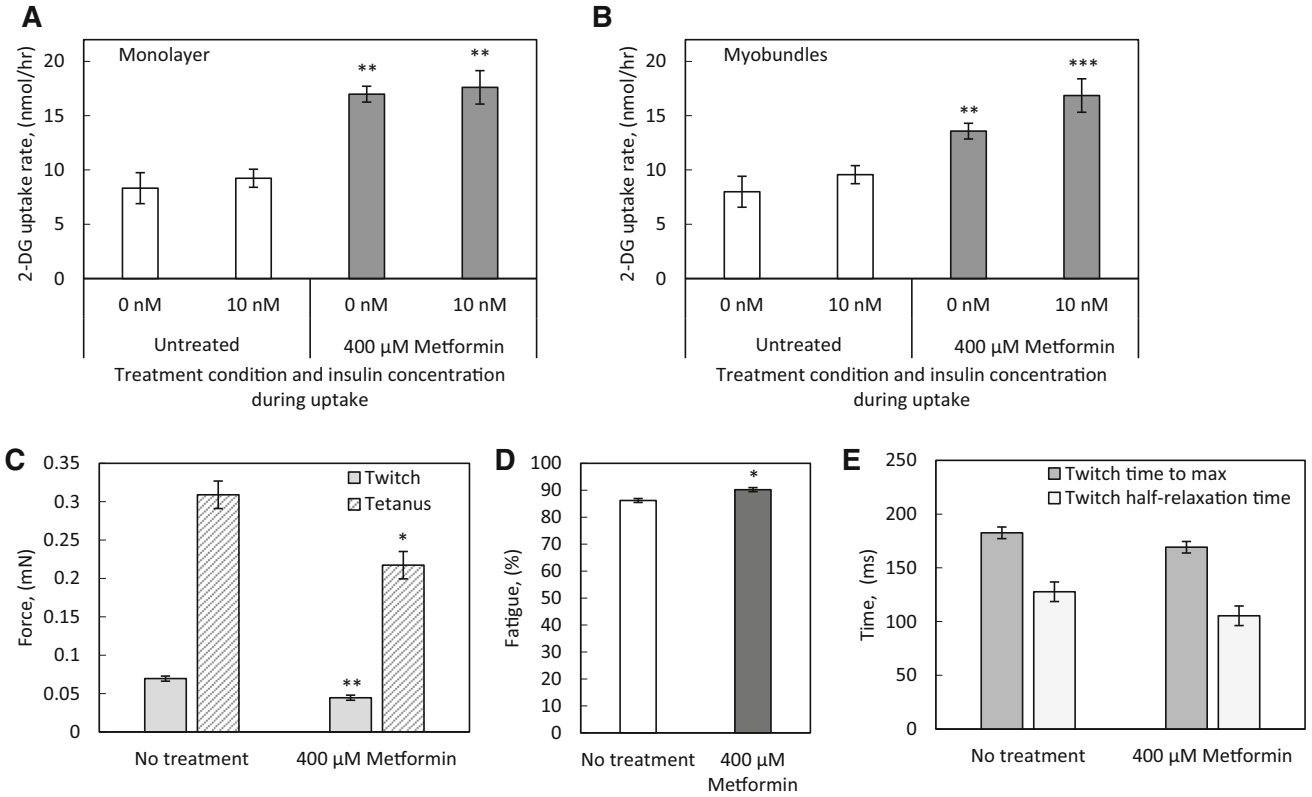

Fig. 3 Effect of metformin treatment on myotube and myobundle function. **A** Myotubes were differentiated in a 6-well plate and treated with 400 µM metformin for 18 h immediately prior to 2-DG uptake at the 2 week differentiation time point. N = 3 donors, n = 3 wells per condition per donor. **B** Myobundles were treated with 400 µM metformin for 18 h immediately prior to 2-DG uptake at the 2 week differentiation time point. N = 3 donors, n = 3−4 myobundles per condition per donor. **C**, **D** Myobundles were treated with 400 µM metformin for 18 h immediately prior to measuring twitch and tetanus contractile force and percent fatigue at the 2 week differentiation time point. N = 3 donors, n = 3-4 myobundles per condition per donor. E) Analysis of time to maximum force and half-relaxation time of twitch contractions. N = 3 donors, n = 3−4 myobundles per condition per donor. * $p < 0.05$, ** $p < 0.01$, *** $p < 0.001$ when compared with the same insulin condition or contractile function measurement in the no treatment group. Data in all panels presented as mean ± S.E.M

isoforms, with lower expression levels of the fast twitch type IIX (MYH1) and immature embryonic (MYH3) and perinatal (MYH8) isoforms (Fig. 4D).

In myotubes in monolayer culture, 18 h of 5 mM 4-PBA treatment resulted in a non-significant trend to increased insulin-stimulated 2-DG uptake, with magnitude of insulin response of 1.1-fold in the untreated group and 1.5-fold in the 4-PBA treated group (Fig. 5A). The 4-PBA-treated myobundles exhibited significantly increased 2-DG uptake after insulin stimulation, with a magnitude of insulin response of 1.2-fold in the untreated group and 1.4-fold in the 4-PBA treated group (Fig. 5B). 4-PBA treatment also enhanced twitch and tetanus force production, though the effect was not statistically significant (Fig. 5C) and resulted in a significant decrease in fatigue following 30 s of electrical stimulation (Fig. 5D), while also significantly lengthening the half-relaxation time of the myobundles during twitch contractions (Fig. 5E).

Analysis of gene expression of glucose transporters revealed decreased GLUT1 gene expression and increased GLUT4 gene expression by myobundles treated with 4-PBA (Fig. 6A). These changes in glucose transporter expression were accompanied by a significant increase in expression of PGC-1α (Fig. 6A). Interestingly, despite gene expression analysis showing decreased GLUT1 expression and increased GLUT4 expression, Western blots showed increased GLUT1 protein expression and decreased GLUT4 protein expression in 4-PBA-treated myobundles (Fig. 6B, C). Treatment with 4-PBA also elicited significant drops in the gene expression of the slow type I MHC isoform (MYH7) as well as a greater drop in the fast type IIX MHC isoform (MYH1) and the immature perinatal isoform (MYH8) (Fig. 6D).

4 Discussion

The goal of this work was to characterize the glucose uptake and insulin sensitivity of three-dimensional human myobundles and to test the ability of the system to respond

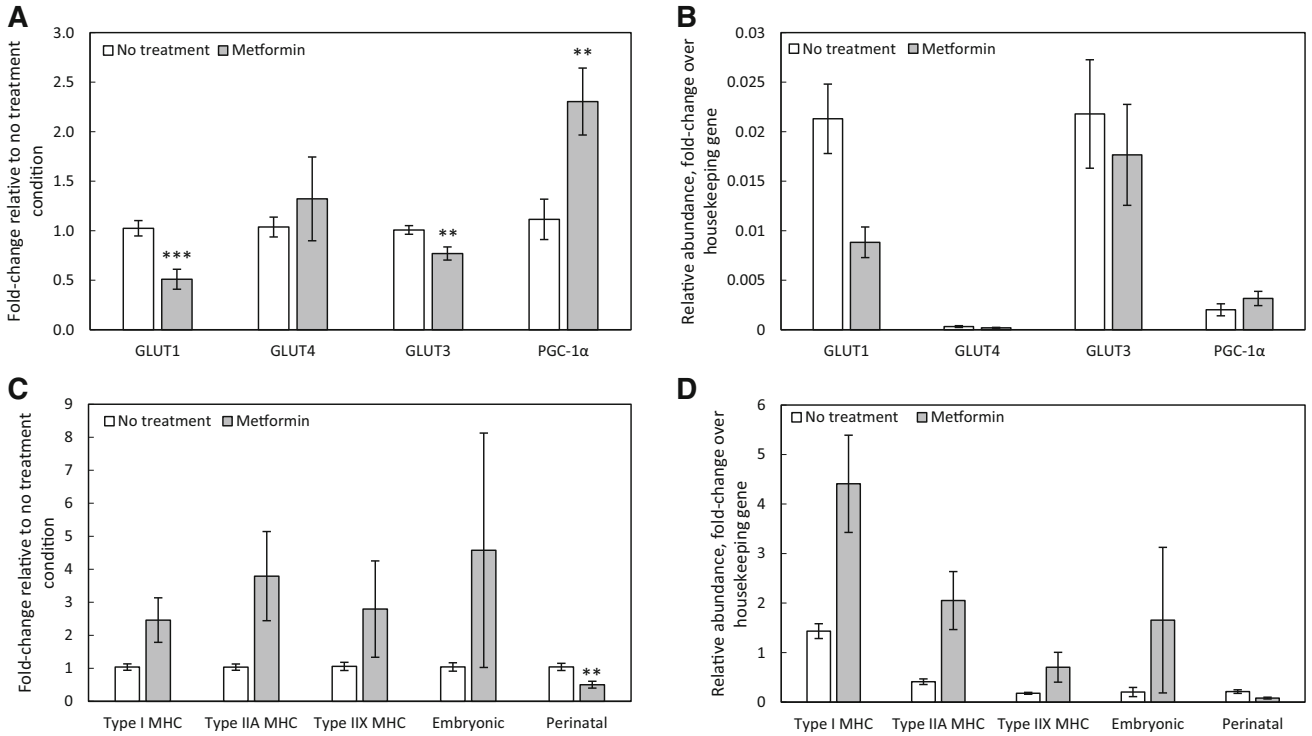

Fig. 4 Effect of metformin treatment on myobundle gene expression. Myobundles were treated with 400 μM metformin for 18 h immediately prior to flash freezing. Gene expression of **A**, **B** glucose transporters GLUT1, GLUT4, and GLUT3 and metabolic regulator PGC-1α and **C**, **D** myosin heavy chain isoforms was determined. For all panels, N = 3 donors, n = 3 myobundles per treatment condition per donor. $^{**}p < 0.01$, $^{***}p < 0.001$ when compared with the no treatment group. Data in all panels presented as mean ± S.E.M

appropriately to a drug challenge known to alter glucose uptake. We found that the magnitude of the insulin response in myobundles is comparable to that of other in vitro skeletal muscle cultures, but myobundles retain the insulin sensitivity of in vivo muscle. Myobundles responded to metformin with a robust increase in 2-DG uptake, indicating the functionality of AMPK-mediated signaling pathways. Finally, we found that pan HDAC inhibition improved the insulin response and contractile function of the myobundles.

To determine the magnitude of change in 2-DG uptake upon exposure to insulin and to characterize the sensitivity of the myobundles to insulin, we measured 2-DG uptake at a variety of insulin concentrations in four donors. The magnitude of the response to physiological insulin concentrations was variable between donors, ranging from 1.2-fold to 2.28-fold, with a compiled response of 1.5 ± 0.2-fold. These values are in the range of what has typically been measured using in vitro human myotubes, with the magnitude of the insulin response ranging from 1.3–3-fold [34–38], but in vivo, the magnitude of change in glucose uptake in response to insulin ranges from six–eight-fold [39–42].

While the magnitude of insulin responsiveness of myobundles remains lacking when compared with reported in vivo values, we hypothesized that the improved physiological relevance of the three-dimensional structure could contribute to greater insulin responsiveness by myobundles than by myotubes in monolayer culture. After culturing cells from several donors in either the myobundle system or in monolayer culture, three-dimensional myobundles exhibited a significantly increased insulin response when compared with the monolayer cultures from the same set of donors. Additionally, the EC_{50} was 0.27 ± 0.03 nM for insulin-mediated glucose uptake. Others have reported EC_{50} values of 3.5 nM [34], 1.0 ± 0.1 nM [37], and 1.6 ± 0.5 nM [36] for human cultured myotubes isolated from healthy subjects. The concentration at which insulin's effect is half-maximal in vivo is reported as 60 μU/mL [43], or 0.36 nM. Thus, the insulin sensitivity of myobundles in vitro is greater than that of the reported sensitivity in monolayer cultures, and more closely matches the sensitivity of skeletal muscle in vivo. Together with the finding of a greater response to 10 nM insulin in myobundles than in monolayer myotubes, these results support the hypothesis that providing cells with a three-dimensional environment can promote improvements in in vitro cultured skeletal muscle relevance to physiologic function.

In vivo, metformin treatment causes a drop in blood glucose concentration of 1.2 mM, an approximate 1.25-

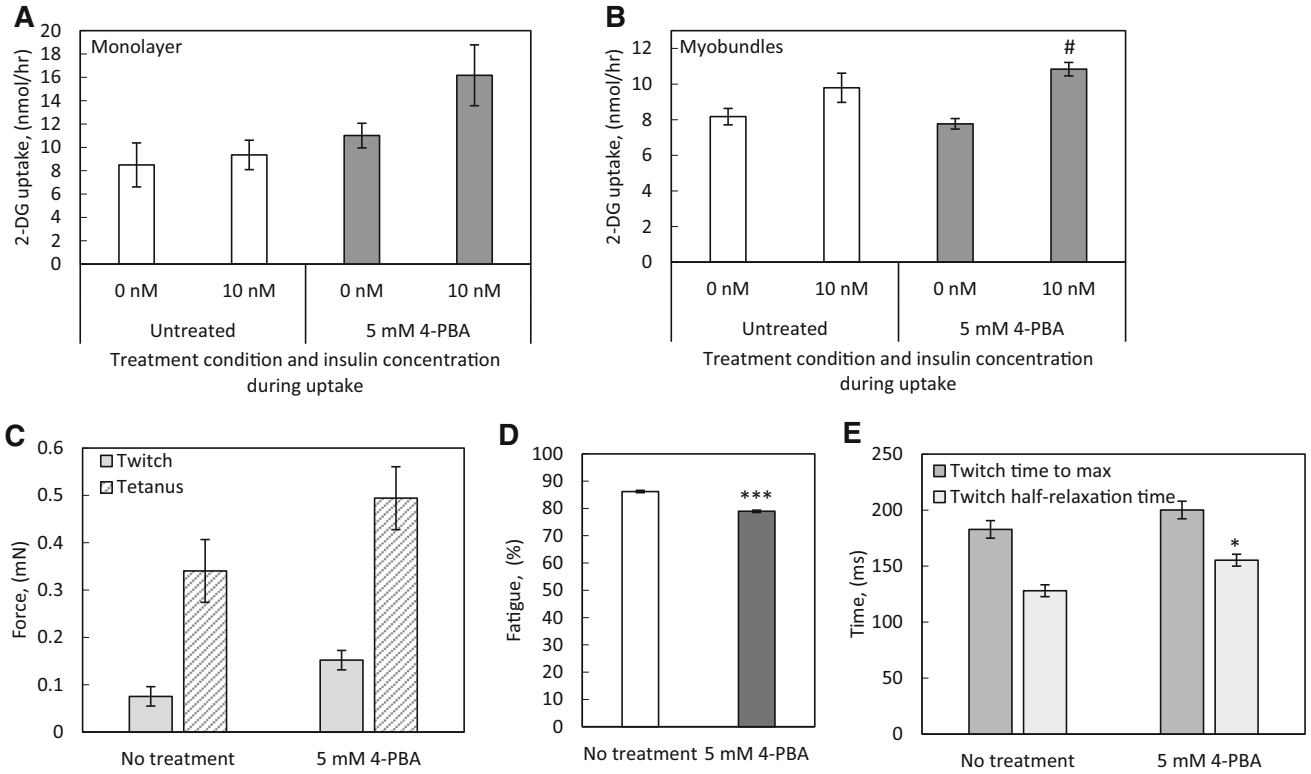

Fig. 5 Effect of the general HDAC inhibitor 4-PBA on myotube and myobundle function. **A** Myotubes were differentiated in a 6-well plate and treated with 5 mM 4-PBA for 18 h immediately prior to 2-DG uptake at the 2 week differentiation time point. N = 3 donors, n = 3 wells per condition per donor. **B** Myobundles were treated with 5 mM 4-PBA for 18 h immediately prior to 2-DG uptake at the 2 week differentiation time point. N = 3 donors, n = 3−4 myobundles per condition per donor. **C**–**E** Myobundles were treated with 5 mM 4-PBA for 18 h immediately prior to measuring twitch and tetanus contractile force, percent fatigue, and twitch kinetics at the 2 week differentiation time point. N = 3 donors, n = 3−4 myobundles per condition per donor. For all panels, N = 3 donors, n = 3 myobundles per condition per donor. $*p < 0.05$, $**p < 0.01$, $***p < 0.001$ when compared with the same insulin condition or contractile function measurement in the no treatment group.# $p < 0.05$ when compared with the no insulin condition within the treatment group. Data in all panels presented as mean ± S.E.M

fold decrease [44], and in type 2 diabetes subjects, long term treatment with metformin increases whole-body glucose disposal by 1.22-fold [45]. Metformin does not enhance insulin-mediated glucose uptake in peripheral tissues of type 2 diabetes patients [46] and cultured human myotubes [33], although in muscle strips from non-insulin-dependent diabetes mellitus patients, metformin treatment did enhance insulin-stimulated glucose transport [47]. We found that when the myobundles were treated with metformin, they responded with an approximate 1.7-fold increase in basal 2-DG uptake rate, but did not enhance insulin responsiveness. The effect in myobundles was consistent with the effect we observed in 2D cultures of myotubes and is comparable with other studies done using human myotubes in monolayer, which demonstrate a metformin-induced 1.4-2.2 fold increase in basal glucose uptake [33, 48]. This response to a well-known drug affecting glucose metabolism in skeletal muscle validates the ability of the myobundle system to respond appropriately to a metabolic challenge.

We additionally observed that metformin treatment significantly decreased fatigue resistance and myobundle force production. Metformin activates AMPK by acting as an inhibitor of complex I, the mitochondrial respiratory chain component, and there is some evidence that treatment with metformin reduces aerobic capacity during high intensity exercise [49], but does not affect aerobic capacity during moderate intensity exercise [50]. The concentration of metformin used in this study is far higher than the average therapeutic plasma concentration of 14.3 μM [51], so decreases in contractile function in the myobundles may predict skeletal muscle dysfunction associated with increased respiratory chain disruption at higher doses of metformin. It is also possible that metformin-mediated AMPK activation inhibits mTORC1 [52], resulting in decreased protein synthesis [53, 54] and manifesting as a decline in contractile force production [7, 55].

In human vastus lateralis muscle, the fiber type composition has been measured as 50–55% type I fibers, 30–35% type IIA fibers, and 10–20% type IIX fibers [56].

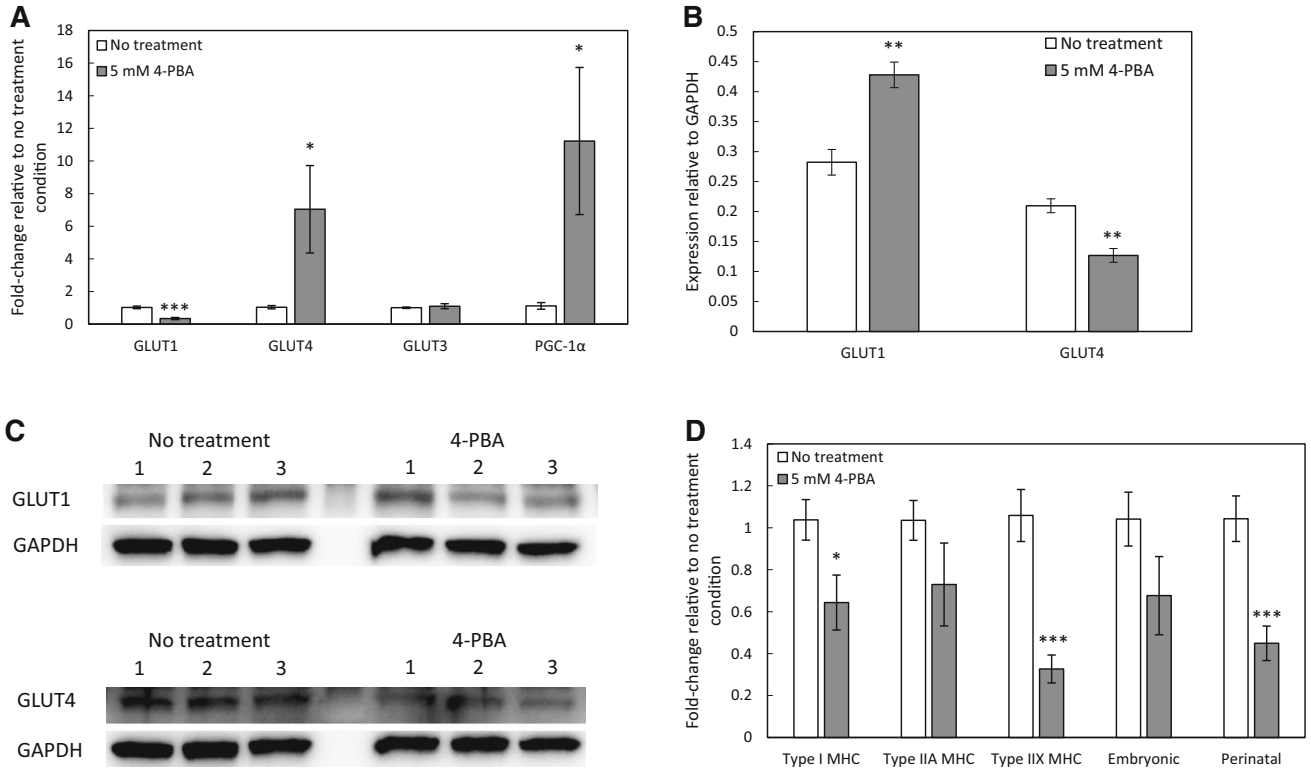

Fig. 6 Effect of 4-PBA treatment on myobundle gene and protein expression. Myobundles were treated with 5 mM 4-PBA for 18 h immediately prior to flash freezing. **A** Gene expression of glucose transporters GLUT1, GLUT4, and GLUT3 and metabolic regulator PGC-1α. N = 3 donors, n = 3 myobundles per treatment condition per donor. **B** Quantification of Western blots for glucose transporters GLUT1 and GLUT4. N = 3 donors, n = 6–9 myobundles per treatment condition per donor. **C** Representative Western blots for one donor. Each lane contains pooled protein from 3 myobundles. **D** Gene expression of myosin heavy chain isoforms. N = 3 donors, n = 3 myobundles per treatment condition per donor. $^{*}p < 0.05$, $^{**}p < 0.01$, $^{***}p < 0.001$ when compared with the no treatment group. Data in all panels presented as mean ± S.E.M

There is a great deal of plasticity in fiber type, with shifts in fiber type enrichment resulting from exercise [57, 58], and disease [59]. In addition to those that are prevalent in adult skeletal muscle, certain myosin heavy chain isoforms are only expressed during development and muscle fiber regeneration [60]. These include MYH3-encoded embryonic MHC and MYH8-encoded perinatal MHC. During early development in humans, embryonic, perinatal, and type I fibers are all present in primary generation fibers [61], with secondary generation fibers expressing only embryonic and perinatal isoforms [62]. Prior to birth, the expression of embryonic and perinatal isoforms declines and the type I isoform reemerges [63]. After injury to adult muscle, embryonic and perinatal MHC isoforms are again detectable in regenerating myofibers [64]. In the untreated state, myobundles expressed the type I isoform in the greatest abundance, followed by type IIA, then perinatal and embryonic, and finally type IIX. The presence of immature isoforms, which has been previously observed in human myobundles [65], suggests that myobundles are representative of either early development or regenerating muscle.

The general HDAC inhibitor 4-PBA [66] inhibits all class IIa HDACs. In C2C12 cells, 4-PBA increased insulin-stimulated glucose uptake and increased GLUT4 expression via inhibition of HDAC5-mediated repression of MEF2 [67]. In our work, acute treatment with 4-PBA after two weeks of differentiation resulted in a trend toward increased force production, and a significant decrease in fatigue. It is likely that the change in twitch kinetics is explained by alterations in calcium handling protein isoform expression, which are impacted by HDAC inhibition in cardiac muscle [68] and have been shown to regulate twitch kinetics in C2C12 [13–15] and human [7] engineered skeletal muscle.

Gene expression data from 4-PBA-treated myobundles indicated decreased GLUT1 and increased GLUT4 expression compared to untreated controls. This shift in glucose transporter expression is potentially mediated by the observed increase in PGC-1α expression, as ectopic expression of PGC-1α has been shown to increase GLUT4 expression in myotubes [69]. However, protein expression analysis indicated increased GLUT1 and decreased GLUT4 protein levels following treatment with 4-PBA, perhaps

reflecting feedback regulation of gene expression. Together, these results suggest that while 4-PBA treatment influences glucose transporter gene expression, the changes in glucose uptake rates in response to HDAC inhibition are occurring by some mechanism other than glucose transporter abundance. One such mode of action could be 4-PBA mediated increased GLUT4 translocation in response to insulin signaling [70], but the effects of the HDAC inhibition are likely to be broad due to the role of HDACs in the regulation of MEF2 [30].

In conclusion, we have characterized the insulin responsiveness and sensitivity of the myobundles, finding insulin responsiveness to be lower than and insulin sensitivity to be comparable to that of skeletal muscle in vivo. Additionally, we validated the ability of the myobundle system to respond appropriately to the metabolic pathway-targeting therapeutic metformin. Finally, we have demonstrated that treatment with a pan-HDAC inhibitor can enhance the metabolic and contractile function of the myobundles. Taken together, we have demonstrated the utility of myobundles as an in vitro tissue-engineered human skeletal muscle model which is valuable for ascertaining both glucose-associated metabolic and contractile functional responses to manipulations of culture conditions and drug treatments.

Acknowledgements This work was supported by the NIH grants UH2TR000505 and UG3TR002412 from NCATS and NIAMS, the NIH Common Fund for the Microphysiological Systems Initiative to GAT, as well as an NSF Graduate Research Fellowship to MEK.

Compliance with Ethical Standards

Conflict of interest The authors have no financial conflicts of interest.

Ethical statement Primary human myogenic cells were isolated from surgical waste samples obtained according to a Duke IRB-approved protocol (IRB No. Pro00063964).

References

1. Janssen I, Heymsfield SB, Wang ZM. Ross R. Skeletal muscle mass and distribution in 468 men and women aged 18–88 yr. J Appl Physiol (1985). 2000;89:81–8.
2. Latroche C, Gitiaux C, Chrétien F, Desguerre I, Mounier R, Chazaud B. Skeletal muscle microvasculature: a highly dynamic lifeline. Physiology (Bethesda). 2015;30:417–27.
3. Collinsworth AM, Zhang S, Kraus WE, Truskey GA. Apparent elastic modulus and hysteresis of skeletal muscle cells throughout differentiation. Am J Physiol Cell Physiol. 2002;283:C1219–27.
4. Madden L, Juhas M, Kraus WE, Truskey GA, Bursac N. Bioengineered human myobundles mimic clinical responses of skeletal muscle to drugs. Elife. 2015;4:e04885.
5. Davis BN, Santoso JW, Walker MJ, Cheng CS, Koves TR, Kraus WE, et al. Human, tissue-engineered, skeletal muscle myobundles to measure oxygen uptake and assess mitochondrial toxicity. Tissue Eng Part C Methods. 2017;23:189–99.
6. Cheng CS, Ran L, Bursac N, Kraus WE, Truskey GA. Cell density and joint microRNA-133a and microRNA-696 inhibition enhance differentiation and contractile function of engineered human skeletal muscle tissues. Tissue Eng Part A. 2016;22:573–83.
7. Khodabukus A, Madden L, Prabhu NK, Koves TR, Jackman CP, Muoio DM, et al. Electrical stimulation increases hypertrophy and metabolic flux in tissue-engineered human skeletal muscle. Biomaterials. 2019;198:259–69.
8. Truskey GA, Achneck HE, Bursac N, Chan H, Cheng CS, Fernandez C, et al. Design considerations for an integrated microphysiological muscle tissue for drug and tissue toxicity testing. Stem Cell Res Ther. 2013;4:S10.
9. Baron AD, Brechtel G, Wallace P, Edelman SV. Rates and tissue sites of non-insulin- and insulin-mediated glucose uptake in humans. Am J Physiol. 1988;255:E769–74.
10. Taniguchi CM, Emanuelli B, Kahn CR. Critical nodes in signalling pathways: insights into insulin action. Nat Rev Mol Cell Biol. 2006;7:85–96.
11. Middelbeek RJ, Chambers MA, Tantiwong P, Treebak JT, An D, Hirshman MF, et al. Insulin stimulation regulates AS160 and TBC1D1 phosphorylation sites in human skeletal muscle. Nutr Diabetes. 2013;3:e74.
12. Baker EL, Dennis RG, Larkin LM. Glucose transporter content and glucose uptake in skeletal muscle constructs engineered in vitro. In Vitro Cell Dev Biol Anim. 2003;39:434–9.
13. Khodabukus A, Baar K. Glucose concentration and streptomycin alter in vitro muscle function and metabolism. J Cell Physiol. 2015;230:1226–34.
14. Khodabukus A, Baar K. The effect of serum origin on tissue engineered skeletal muscle function. J Cell Biochem. 2014;115:2198–207.
15. Khodabukus A, Baehr LM, Bodine SC, Baar K. Role of contraction duration in inducing fast-to-slow contractile and metabolic protein and functional changes in engineered muscle. J Cell Physiol. 2015;230:2489–97.
16. Khodabukus A, Baar K. Contractile and metabolic properties of engineered skeletal muscle derived from slow and fast phenotype mouse muscle. J Cell Physiol. 2015;230:1750–7.
17. Krauss RS, Joseph GA, Goel AJ. Keep your friends close: cell-cell contact and skeletal myogenesis. Cold Spring Harb Perspect Biol. 2017;9:a029298.
18. Lemke SB, Schnorrer F. Mechanical forces during muscle development. Mech Dev. 2017;144:92–101.
19. Ahmad K, Lee EJ, Moon JS, Park SY, Choi I. Multifaceted interweaving between extracellular matrix, insulin resistance, and skeletal muscle. Cells. 2018;7:E148.
20. Williams AS, Kang L, Wasserman DH. The extracellular matrix and insulin resistance. Trends Endocrinol Metab. 2015;26:357–66.
21. Owen MR, Doran E, Halestrap AP. Evidence that metformin exerts its anti-diabetic effects through inhibition of complex 1 of the mitochondrial respiratory chain. Biochem J. 2000;348:607–14.
22. El-Mir MY, Nogueira V, Fontaine E, Avéret N, Rigoulet M, Leverve X. Dimethylbiguanide inhibits cell respiration via an indirect effect targeted on the respiratory chain complex I. J Biol Chem. 2000;275:223–8.
23. Turban S, Stretton C, Drouin O, Green CJ, Watson ML, Gray A, et al. Defining the contribution of AMP-activated protein kinase (AMPK) and protein kinase C (PKC) in regulation of glucose uptake by metformin in skeletal muscle cells. J Biol Chem. 2012;287:20088–99.

24. Gholobova D, Gerard M, Decroix L, Desender L, Callewaert N, Annaert P, et al. Human tissue-engineered skeletal muscle: a novel 3D in vitro model for drug disposition and toxicity after intramuscular injection. Sci Rep. 2018;8:12206.
25. Martin M, Kettmann R, Dequiedt F. Class IIa histone deacetylases: regulating the regulators. Oncogene. 2007;26:5450–67.
26. Dressel U, Bailey PJ, Wang SC, Downes M, Evans RM, Muscat GE. A dynamic role for HDAC7 in MEF2-mediated muscle differentiation. J Biol Chem. 2001;276:17007–13.
27. McKinsey TA, Zhang CL, Lu J, Olson EN. Signal-dependent nuclear export of a histone deacetylase regulates muscle differentiation. Nature. 2000;408:106–11.
28. Lu J, McKinsey TA, Zhang CL, Olson EN. Regulation of skeletal myogenesis by association of the MEF2 transcription factor with class II histone deacetylases. Mol Cell. 2000;6:233–44.
29. Cohen TJ, Choi MC, Kapur M, Lira VA, Yan Z, Yao TP. HDAC4 regulates muscle fiber type-specific gene expression programs. Mol Cells. 2015;38:343–8.
30. Gaur V, Connor T, Sanigorski A, Martin SD, Bruce CR, Henstridge DC, et al. Disruption of the class IIa HDAC corepressor complex increases energy expenditure and lipid oxidation. Cell Rep. 2016;16:2802–10.
31. Yamamoto N, Ueda M, Sato T, Kawasaki K, Sawada K, Kawabata K, et al. Measurement of glucose uptake in cultured cells. Curr Protoc Pharmacol. 2011;55:12.14.1–22. https://doi.org/10.1002/0471141755.ph1214s55.
32. Li G, Barrett EJ, Wang H, Chai W, Liu Z. Insulin at physiological concentrations selectively activates insulin but not insulin-like growth factor I (IGF-I) or insulin/IGF-I hybrid receptors in endothelial cells. Endocrinology. 2005;146:4690–6.
33. Sarabia V, Lam L, Burdett E, Leiter LA, Klip A. Glucose transport in human skeletal muscle cells in culture. Stimulation by insulin and metformin. J Clin Invest. 1992;90:1386–95.
34. Sarabia V, Ramlal T, Klip A. Glucose uptake in human and animal muscle cells in culture. Biochem Cell Biol. 1990;68:536–42.
35. Ciaraldi TP, Abrams L, Nikoulina S, Mudaliar S, Henry RR. Glucose transport in cultured human skeletal muscle cells. Regulation by insulin and glucose in nondiabetic and non-insulin-dependent diabetes mellitus subjects. J Clin Invest. 1995;96:2820–7.
36. Ciaraldi TP, Phillips SA, Carter L, Aroda V, Mudaliar S, Henry RR. Effects of the rapid-acting insulin analog glulisine on cultured human skeletal muscle cells: comparisons with insulin and insulin-like growth factor I. J Clin Endocrinol Metab. 2005;90:5551–8.
37. Henry RR, Abrams L, Nikoulina S, Ciaraldi TP. Insulin action and glucose metabolism in nondiabetic control and NIDDM subjects. Comparison using human skeletal muscle cell cultures. Diabetes. 1995;44:936–46.
38. Al-Khalili L, Chibalin AV, Kannisto K, Zhang BB, Permert J, Holman GD, et al. Insulin action in cultured human skeletal muscle cells during differentiation: assessment of cell surface GLUT4 and GLUT1 content. Cell Mol Life Sci. 2003;60:991–8.
39. DeFronzo RA, Jacot E, Jequier E, Maeder E, Wahren J, Felber JP. The effect of insulin on the disposal of intravenous glucose Results from indirect calorimetry and hepatic and femoral venous catheterization. Diabetes. 1981;30:1000–7.
40. Bonadonna RC, Del Prato S, Saccomani MP, Bonora E, Gulli G, Ferrannini E, et al. Transmembrane glucose transport in skeletal muscle of patients with non-insulin-dependent diabetes. J Clin Invest. 1993;92:486–94.
41. Bonadonna RC, Groop L, Kraemer N, Ferrannini E, Del Prato S, DeFronzo RA. Obesity and insulin resistance in humans: a dose-response study. Metabolism. 1990;39:452–9.
42. Yki-Järvinen H, Young AA, Lamkin C, Foley JE. Kinetics of glucose disposal in whole body and across the forearm in man. J Clin Invest. 1987;79:1713–9.
43. Abdul-Ghani MA, DeFronzo RA. Pathogenesis of insulin resistance in skeletal muscle. J Biomed Biotechnol. 2010;2010:476279.
44. Popov DV, Lysenko EA, Butkov AD, Vepkhvadze TF, Perfilov DV, Vinogradova OL. AMPK does not play a requisite role in regulation of PPARGC1A gene expression via the alternative promoter in endurance-trained human skeletal muscle. Exp Physiol. 2017;102:366–75.
45. Kim YB, Ciaraldi TP, Kong A, Kim D, Chu N, Mohideen P, et al. Troglitazone but not metformin restores insulin-stimulated phosphoinositide 3-kinase activity and increases p110beta protein levels in skeletal muscle of type 2 diabetic subjects. Diabetes. 2002;51:443–8.
46. Natali A, Ferrannini E. Effects of metformin and thiazolidinediones on suppression of hepatic glucose production and stimulation of glucose uptake in type 2 diabetes: a systematic review. Diabetologia. 2006;49:434–41.
47. Galuska D, Nolte LA, Zierath JR, Wallberg-Henriksson H. Effect of metformin on insulin-stimulated glucose transport in isolated skeletal muscle obtained from patients with NIDDM. Diabetologia. 1994;37:826–32.
48. Brown AE, Dibnah B, Fisher E, Newton JL, Walker M. Pharmacological activation of AMPK and glucose uptake in cultured human skeletal muscle cells from patients with ME/CFS. Biosci Rep. 2018;38:BSR20180242.
49. Braun B, Eze P, Stephens BR, Hagobian TA, Sharoff CG, Chipkin SR, et al. Impact of metformin on peak aerobic capacity. Appl Physiol Nutr Metab. 2008;33:61–7.
50. Das S, Behera SK, Srinivasan A, Xavier AS, Selvarajan S, Kamalanathan S, et al. Effect of metformin on exercise capacity: a meta-analysis. Diabetes Res Clin Pract. 2018;144:270–8.
51. Hess C, Unger M, Madea B, Stratmann B, Tschoepe D. Range of therapeutic metformin concentrations in clinical blood samples and comparison to a forensic case with death due to lactic acidosis. Forensic Sci Int. 2018;286:106–12.
52. Gwinn DM, Shackelford DB, Egan DF, Mihaylova MM, Mery A, Vasquez DS, et al. AMPK phosphorylation of raptor mediates a metabolic checkpoint. Mol Cell. 2008;30:214–26.
53. Drummond MJ, Fry CS, Glynn EL, Dreyer HC, Dhanani S, Timmerman KL, et al. Rapamycin administration in humans blocks the contraction-induced increase in skeletal muscle protein synthesis. J Physiol. 2009;587:1535–46.
54. Horman S, Browne G, Krause U, Patel J, Vertommen D, Bertrand L, et al. Activation of AMP-activated protein kinase leads to the phosphorylation of elongation factor 2 and an inhibition of protein synthesis. Curr Biol. 2002;12:1419–23.
55. Khodabukus A, Baar K. Defined electrical stimulation emphasizing excitability for the development and testing of engineered skeletal muscle. Tissue Eng Part C Methods. 2012;18:349–57.
56. Egan B, Zierath JR. Exercise metabolism and the molecular regulation of skeletal muscle adaptation. Cell Metab. 2013;17:162–84.
57. Gollnick PD, Armstrong RB, Saltin B, Saubert CW 4th, Sembrowich WL, Shepherd RE. Effect of training on enzyme activity and fiber composition of human skeletal muscle. J Appl Physiol. 1973;34:107–11.
58. Anderson RM, Weindruch R. Metabolic reprogramming, caloric restriction and aging. Trends Endocrinol Metab. 2010;21:134–41.
59. Talbot J, Maves L. Skeletal muscle fiber type: using insights from muscle developmental biology to dissect targets for susceptibility and resistance to muscle disease. Wiley Interdiscip Rev Dev Biol. 2016;5:518–34.

60. Schiaffino S, Rossi AC, Smerdu V, Leinwand LA, Reggiani C. Developmental myosins: expression patterns and functional significance. Skelet Muscle. 2015;5:22.
61. Barbet JP, Thornell LE, Butler-Browne GS. Immunocytochemical characterisation of two generations of fibers during the development of the human quadriceps muscle. Mech Dev. 1991;35:3–11.
62. Cho M, Webster SG, Blau HM. Evidence for myoblast-extrinsic regulation of slow myosin heavy chain expression during muscle fiber formation in embryonic development. J Cell Biol. 1993;121:795–810.
63. Draeger A, Weeds AG, Fitzsimons RB. Primary, secondary and tertiary myotubes in developing skeletal muscle: a new approach to the analysis of human myogenesis. J Neurol Sci. 1987;81:19–43.
64. Sartore S, Gorza L, Schiaffino S. Fetal myosin heavy chains in regenerating muscle. Nature. 1982;298:294–6.
65. Davis BNJ, Santoso JW, Walker MJ, Oliver CE, Cunningham MM, Boehm CA, et al. Modeling the Effect of TNF-alpha upon Drug-Induced Toxicity in Human. Tissue-Engineered Myobundles. Ann Biomed Eng. 2019;47:1596–610.
66. Koutsounas I, Giaginis C, Theocharis S. Histone deacetylase inhibitors and pancreatic cancer: are there any promising clinical trials? World J Gastroenterol. 2013;19:1173–81.
67. Hu H, Li L, Wang C, He H, Mao K, Ma X, et al. 4-Phenylbutyric acid increases GLUT4 gene expression through suppression of HDAC5 but not endoplasmic reticulum stress. Cell Physiol Biochem. 2014;33:1899–910.
68. Meraviglia V, Bocchi L, Sacchetto R, Florio MC, Motta BM, Corti C, et al. HDAC inhibition improves the sarcoendoplasmic reticulum Ca^{2+}-ATPase activity in cardiac myocytes. Int J Mol Sci. 2018;19:E419.
69. Michael LF, Wu Z, Cheatham RB, Puigserver P, Adelmant G, Lehman JJ, et al. Restoration of insulin-sensitive glucose transporter (GLUT4) gene expression in muscle cells by the transcriptional coactivator PGC-1. Proc Natl Acad Sci U S A. 2001;98:3820–5.
70. Takigawa-Imamura H, Sekine T, Murata M, Takayama K, Nakazawa K, Nakagawa J. Stimulation of glucose uptake in muscle cells by prolonged treatment with scriptide, a histone deacetylase inhibitor. Biosci Biotechnol Biochem. 2003;67:1499–506.